Electronics and Communications in Japan, Part 1, Vol. 90, No. 9, 2007
Translated from Denshi Joho Tsushin Gakkai Ronbunshi, Vol. J89-B, No. 9, September 2006, pp. 1776–1788

MIMO-STBC Scheme for Intervehicle Communications Using Decision Feedback Channel Estimation Method Based on Propagation Feature at Intersection

Kenji Ito,[1] Nobuo Itoh,[1] Katsushi Sanda,[1] and Yoshio Karasawa[2]

[1]Toyota Central Research and Development Laboratories, Inc., Aichi, 480-1192 Japan

[2]Advanced Wireless Communication Research Center, The University of Electro-Communications, Chofu, 182-8585 Japan

SUMMARY

This paper investigates an intervehicle communication method as a safe driving support system for intersection collision avoidance warnings. In this kind of system, realization of highly reliable communications in the physical layer is an absolute requirement. As a result, we propose a new MIMO-STBC (Space-Time Block Coding) method based on intersection propagation channel characteristics. MIMO transmission characteristics are determined by the propagation channel characteristics. First, we use a ray-tracing method simulation to clarify the propagation channel conditions, and then model the intersection propagation channel. We use the characteristics of this propagation channel to propose a MIMO-STBC method that utilizes decision feedback channel estimation, and verify the effectiveness of the proposed method in computer simulations. © 2007 Wiley Periodicals, Inc. Electron Comm Jpn Pt 1, 90(9): 1–15, 2007; Published online in Wiley InterScience (www.interscience.wiley.com). DOI 10.1002/ecja.20400

Key words: MIMO; Intelligent Transport Systems; intervehicle communication; decision feedback channel estimation; space-time block coding.

1. Introduction

Seatbelts, airbags, and other passive safety technologies are extremely important in reducing the number of deaths and injuries due to automobile accidents. Now there are expectations for active safety technologies such as VSC (Vehicle Safety Communications) for avoiding accidents, and various researches are in progress [1]. While cameras or radar are already used in forward obstacle collision prevention support systems, etc., issues have been raised where these on-board sensors alone do not demonstrate sufficient effectiveness as systems, in environments where obstacles exist outside of the visible range.

For this issue, great expectations have been raised in the VSC research sector for a collision avoidance warning system using Inter-Vehicle Communication (IVC) like that shown in Fig. 1. This involves an exchange of multipoint-to-multipoint communications between vehicles at intersections or hidden driveways regarding approach information for both vehicles (such as position information, speed information, etc.), and to then send warnings to the drivers that lead to avoidance of the collision. In the future, links to the vehicle control systems could also lead to achievement of vehicle stops and other automatic controls. In this paper, for the first step in this investigation we shall target point-to-point communication systems, in which each vehicle comes into an intersection from a direction outside the line-of-sight.

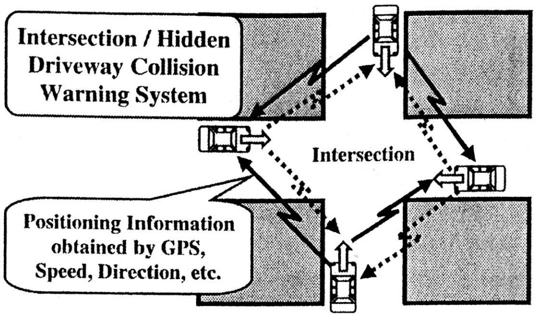

Fig. 1. System image of collision avoidance warning using IVC.

Realization of a safe driving support system using this kind of communication demands high reliability in the higher layer of communication. Therefore, assurance of the possibility of communication at the physical layer is essential even in communication environments without line-of-sight. At present, attention is focused on MIMO (Multiple-Input Multiple-Output) technology, which uses array antennas for both transmitting and receiving, as one element technology for improving reliability at the physical layer. There has been much research and development in this area in recent years, as a technology for improving the communications quality of wireless communications systems in environments where multi-paths exist due to reflections and scattered waves, etc., and for enabling high-speed large-capacity communications [2].

Moreover, since a key transmission feature of MIMO systems is determined by the target propagation characteristics, research on modeling the MIMO propagation channel is also being actively pursued [3–5]. However, investigations into application of MIMO transmission IVC that take the intersection propagation model into consideration are virtually nonexistent.

Therefore, we take into consideration the radio propagation conditions during IVC at intersections to investigate the optimum communication method using application of the MIMO system. MIMO can be classified by system configuration depending on the usage objective (higher-speed larger-capacity transmission and higher reliability: SNR improvement) and the existence of propagation channel information (CSI: Channel State Information). Safe driving support systems demand reliability over high transmission capacity, and also require real-time capability. In addition, since accurate estimation of CSI for both transmitting and receiving requires two-way communication, the control methods and other system configurations become quite complex.

In this paper, therefore, for the achievement of higher reliability we investigate application of a MIMO-STBC method that makes use of Space-Time Block Coding (STBC) using CSI for receiving only [6]. The STBC method requires accurate propagation channel estimation. In IVC, however, movement of the transmitting and receiving terminal risks causing an error in propagation channel estimation, resulting in deterioration of communication quality. Since these kinds of characteristics are determined by the propagation channel characteristics, we first examine the propagation channel response characteristics (e.g., the channel impulse responses) in the intersection model.

For complex layouts such as intersections, we consider the ray-tracing method to be effective as a method for estimating propagation channel characteristics. The ray-tracing method merely finds the geometrical track between transmitting and receiving, and is used as a method for relatively simple estimation of electric field intensities [7, 8]. Therefore, it should easily be able to find propagation channel characteristics, as well. We also propose an IVC method using a decision feedback channel estimation method suitable for propagation channel response characteristics, and use a computer simulation to clarify its validity.

The rest of the paper is organized as follows. In Section 2 we describe the problems with the MIMO-STBC method in the target application model and in fast fading environments, while in Section 3 we explain the intersection propagation simulation using the ray-tracing method, and show the evaluation results. Next, in Section 4 we model the intersection propagation channel, based on the propagation characteristic evaluation results. Then, in Section 5 we give an overview of the proposed method using the decision feedback channel estimation method applied to the intersection propagation channel characteristics. Furthermore, in Section 6 we explain the statistical evaluation method in the computer simulation, and show the evaluation results for the proposed method.

2. Problems with MIMO-STBC in Fast Fading Environments

In IVC where both the transmitting and receiving terminals are moving, communication is occurring in a fast fading environment. In this section, we first give an overview of the system configuration using the MIMO-STBC method, and then move to an overview of the communication preconditions in the target application, and the problems with MIMO-STBC in a fast fading environment.

2.1. Basic concept of MIMO-STBC method

In this paper, we adopt a 2×2 MIMO system, which realizes full-rate and full-diversity performance as shown in Fig. 2. The propagation channel matrix $\mathbf{H}(t_0)$ at time t_0, and the STBC matrix $\mathbf{G}_2(m)$ for discrete time $2m$ and $2m + 1$, can be expressed as follows:

$$\mathbf{H}(t_0) = \begin{bmatrix} h_{11} & h_{12} \\ h_{21} & h_{22} \end{bmatrix} \tag{1}$$

$$\mathbf{G}_2(m) = \begin{bmatrix} s(2m) & s(2m+1) \\ -s^*(2m+1) & s^*(2m) \end{bmatrix} \tag{2}$$

Here, the asterisk represents the complex conjugate operation.

The transmitted signals $s(2m)$ and $s(2m + 1)$ are encoded in STE (Space-Time Encoding) according to $\mathbf{G}_2(m)$. The received signals $y_i(2m)$ and $y_i(2m + 1)$ at the i-th receiving antenna are decoded in STD (Space-Time Decoding) using estimation $\hat{\mathbf{H}}$ of the propagation channel $\mathbf{H}(t_0)$. If there is no propagation channel estimation error, then $s(2m)$ and $s(2m + 1)$ can be separately received without mutual interference.

2.2. Application model and problems with MIMO-STBC

In this paper, we target the preventive safety application in intersections. In this kind of application, we need to assume that multiple vehicles exist in the intersection simultaneously and that they are exchanging information with each other. This communication requires that information transmission delays be ensured so as to obtain certain communications. Although the amount of communication per event is small, the information transferred needs to be certain for all vehicles existing near the intersection. In other words, the required characteristics are real-time, low delay capability, and high reliability, and the ideal is packet communication where one vehicle monopolizes the wireless communication for a short period (assumed to be a maximum of 1 ms or less). As a result, we also assume that the pilot signal and other preambles are short (several tens of microseconds, or 16 μs, etc.), and for our system target a semisynchronous detection method that does not reproduce the carrier.

However, when transmitting packet data like that shown in Fig. 3, even if we assume a propagation channel in which the pilot signal has transmit and receive signals that are pre-known (such as Walsh codes), there will be a delay until the packet data can be decoded. In cases where there are huge changes over time in the propagation environment, this delay time could threaten to have an effect on characteristics. In particular, in cases such as IVC where both the transmitter and receiver are in motion, even a short movement will cause the propagation channel to change radically. In other words, an error appears in the characteristics between the propagation channel estimation value based on the pilot signal, and the propagation channel at the time the packet data is received, which leaves behind an interference component between decoded signals after STBC decoding that can degrade reception quality.

For example, the propagation channel matrix $\mathbf{H}(t_0 + \Delta t)$ in the time $(t_0 + \Delta t)$ can be expressed as follows:

$$\begin{aligned} \mathbf{H}(t_0 + \Delta t) &= \begin{bmatrix} \tilde{h}_{11} & \tilde{h}_{12} \\ \tilde{h}_{21} & \tilde{h}_{22} \end{bmatrix} \\ &= \begin{bmatrix} h_{11} + \Delta h_{11} & h_{12} + \Delta h_{12} \\ h_{21} + \Delta h_{21} & h_{22} + \Delta h_{22} \end{bmatrix} \\ &= \mathbf{H}(t_0) + \mathbf{\Delta H}(\Delta t) \end{aligned} \tag{3}$$

Here $\mathbf{\Delta H}(\Delta t)$ represents the propagation channel error component in the change over time Δt.

If we assume that the propagation channel at time t_0 was accurately estimated, then we can express the propagation channel estimate as $\hat{\mathbf{H}} = \mathbf{H}(t_0)$. Therefore, the effects of intersymbol interference (ISI) due to this propagation channel error matrix $\mathbf{\Delta H}$ are received, preventing accurate STBC decoding of the received signal and resulting in a receive error [9].

In Ref. 9, the countermeasure for the case where the dominant radio wave arrival (radiation) direction is the vehicle's forward motion direction, and where the angular spread is small, is to derive an approximation formula capable of expressing the propagation channel by executing phase rotation relative to the movement distance of the

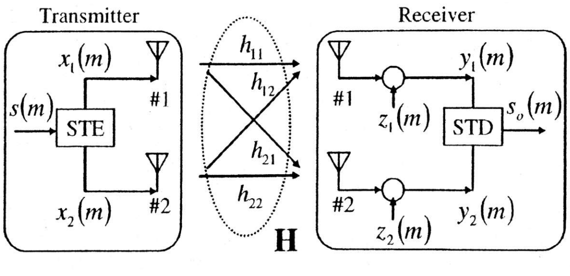

Fig. 2. System model of 2 × 2 MIMO-STBC.

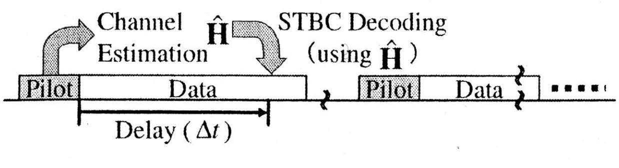

Fig. 3. Packet format for short-packet communication.

transmitting and receiving vehicles. As a result, the transmitting and receiving vehicles utilize the speed information for each vehicle to achieve communication in semistatic conditions, to prevent the ISI error. However, this approximation formula may not work in cases where the radio wave arrival (radiation) direction is at an angle to the vehicle's forward motion direction, or where the angular spread is large.

There have been various investigations into this kind of phase correction in MIMO systems [10–14].

In Ref. 10, for example, the transmit and receive sides detect phase differences between a succession of pre-known pilot signal symbols to achieve phase synchronization of the MIMO system. However, in the safe driving support application targeted in this paper for investigation, we consider the case of bursts of information transmission. As a result, since packets will not necessarily always be sent in succession, we cannot use a method designed like this one to detect phases between continuous pilot signals.

In addition, in Refs. 11 to 13, the transmitter and receiver estimate and correct the amount of phase change within a pre-known single training signal symbol (such as a pilot signal). However, in applications where the pilot signal is short, the accuracy of the estimated phase rotation can be expected to deteriorate. Moreover, while the correction could continue if the phase were to rotate at the same speed until the next pilot signal is received, it is actually highly likely that there will be a major change in the phase rotation during the interval, since in IVC both the transmitter and receiver are in motion. Furthermore, while Ref. 13 shows a relationship between the STBC block length and the estimation accuracy, it is difficult with the length of our pilot signal to obtain sufficient estimation accuracy. As a result, these methods will not necessarily always be able to accurately correct the phase rotation of data areas between successive pilot signals.

Meanwhile, on the receiving side a method has been proposed that calls for STBC encoding with delay detection without use of CSI [15]. In this method, however, the characteristics for SNR deteriorate by just 3 dB compared to synchronous detection, a serious drawback.

Another method that could be considered involves insertion of multiple pilot signals into a packet and performing propagation channel estimation over a short time interval. But using this method is difficult for the short packet communications that we are targeting, because insertion of pilot signals would reduce the amount of data sent, resulting in lower efficiency.

Also, Ref. 14 feeds back the decision signal and calculates complex correlation between the signal and received signal to estimate the amount of phase change. However, this is not necessarily always the most efficient method because it individually estimates the amount of the MIMO channel phase correction between all transmitting and receiving antennas without taking into consideration the propagation channel characteristics.

As can be seen, there are hardly any investigations targeting highly reliable safe driving support applications that take propagation channel characteristics into consideration for efficient phase correction of MIMO systems. As a result, in this paper, for short packet communication like that shown in Fig. 3, we propose a decision feedback channel estimation method that takes into consideration the intersection propagation channel characteristics.

Since the proposed decision feedback channel estimation method incorporates a feedback system signal process, a process delay will always occur. Nevertheless, since we can assume that this process delay will involve an extremely small delay compared to the real-time capability demanded by the application (assuming a tolerated delay of 100 ms or less), we believe that it satisfies applicability for this kind of application. First, therefore, we will evaluate the transmission characteristics for a specific intersection model.

3. Evaluation of Propagation Channel Characteristics Using the Ray-Tracing Method

MIMO transmission characteristics are determined by the propagation channel characteristics. Therefore, in order to survey the propagation environment in an intersection targeted for evaluation, we perform a simulation using the ray-tracing method based on geometric optical theory [7] to trace the radio waves from the transmission point to the reception point.

3.1. Evaluation model

The intersection model for performance evaluation is shown in Fig. 4. The intersection model is assumed to be a 300-m square with road widths of 10 m and office buildings lining the roads, and concrete blocks 10 m high that are randomly positioned. We set the initial positions of both the transmitting point (Tx) and receiving point (Rx) antennas at a distance of 40 m from the road intersection. Since the average stoppable distance for an automobile moving at 60 km/h is assumed to be 40 m, we chose this position as the initial communication position. We assume a road environment where it is impossible to judge which of the vehicles is on the higher priority or lower priority road. We also targeted for evaluation a situation where the signal receiving vehicle is running on the lower priority road, and the initial communication occurs when Rx is at a position 5 m from the intersection. In this case, we consider an application where the signal receiving vehicle running on the lower

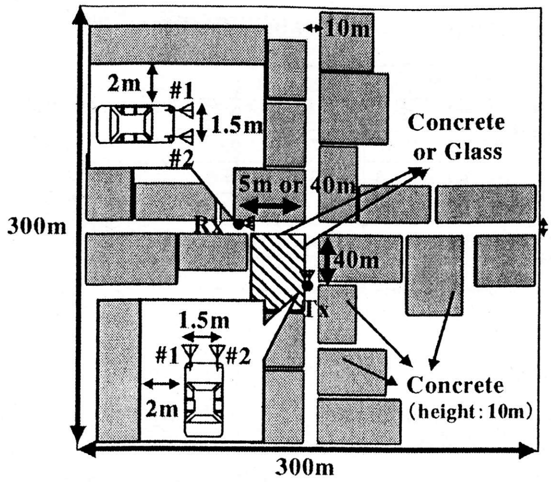

Fig. 4. Intersection model for performance evaluation.

priority road is assumed to be required to stop temporarily immediately before intruding into the higher priority road, and that the vehicle will stop and not intrude into the higher priority road if it has received a vehicle approaching warning from the transmitting vehicle, in order to avoid an accident.

For the transmitting and receiving antenna, we used two standard dipole antennas for each, with the interval between antenna elements of 1.5 m and an antenna height of 0.8 m, and assumed that the antenna axis is perpendicular to the ground surface. In addition, we assumed a distance of 2 m from the wall. Also, we performed the simulation with Tx and Rx traveling at the same speed, and with each moving toward the road intersection.

3.2. Simulation method

For the simulation, we used the ray-tracing software RapLab [16]. This software uses imaging methods to calculate reflection, permeation, and diffraction from the transmitting point, the receiving point, and combinations of all other reflecting surfaces. For the reflection and permeation coefficients, we used the Fresnel coefficient, while for the diffraction coefficient, we used UTD (Uniform Geometric Theory of Diffraction). In the simulation, we changed the maximum reflection coefficient by 1 to 4 times (called, respectively, Case 1, 2, 3, and 4), set the maximum number of diffractions to two times, and also took into consideration reflections off the ground. We limited consideration of the permeation path to direct waves only, and assumed that the block walls existing along the direct line between the transmitting and receiving points were made of glass (the walls along the diagonal lines in Fig. 4). Here we used the values shown in Table 1 for the electrical

Table 1. Electric characteristics of concrete, glass, and ground

Material	Permittivity [F/m]	Conductivity [S/m]	Permeability [H/m]
Concrete	5.99×10^{-11}	2.3×10^{-3}	1.26×10^{-6}
Glass	4.43×10^{-11}	1.0×10^{-12}	1.26×10^{-6}
Ground	2.66×10^{-11}	1.0×10^{-4}	1.26×10^{-6}

characteristics of concrete, glass, and the ground [8, 17]. In addition, for the simulation transmission frequency, we used 6 GHz.

Moreover, as shown in Table 2, for reflection and diffraction only we targeted three evaluation models (Model 1, 2, and 3), including two different initial communication distances (40 m and 5 m) from the intersection to the receiving point, and a case considering direct wave permeation.

Furthermore, to evaluate the MIMO transmission characteristics, we used Eqs. (4) to (6) below to find the propagation channel response matrix. The propagation channel characteristic $h_{n_r n_t}$ between the n_t-th transmitting antenna and the n_r-th receiving antenna can be expressed as shown below [7, 18]:

$$h_{n_r n_t} = \sum_i \left(\frac{G(i) e^{(-jks_{i,1})}}{s_{i,1}} \prod_u R_{i,u} \prod_v T_{i,v} \times \prod_l K_{i,l} D_{i,l} e^{(-jks_{i,l+1})} \right) \tag{4}$$

$$G(i) = g_{n_t}(i) g_{n_r}(i) \tag{5}$$

$$K_{i,l} = \sqrt{\frac{s_{i,l}}{(s_{i,l} + s_{i,l+1}) s_{i,l+1}}} \tag{6}$$

Here $R_{i,u}$, $T_{i,v}$, and $D_{i,l}$ are, respectively, the reflection coefficient when the i-th ray is reflected on reflection surface u,

Table 2. Performance evaluation models

Model conditions	Model 1	Model 2	Model 3
Maximum number of reflections	1∼4	1∼4	1∼4
Maximum number of diffractions	2	2	2
Transmission path	—	—	Direct
Distance of Rx from intersection	40 m	5 m	40 m

Table 3. Propagation simulation results at the intersection for maximum number of diffractions

Model	Model 1		Model 2		Model 3	
Maximum number of diffractions	1	2	1	2	1	2
Total number of paths	16	292	20	316	17	293
Average receive level [dBm]	−105.9	−104.1	−84.1	−83.3	−76.6	−76.6
Delay spread [ns]	14.98	15.10	10.25	14.50	4.15	4.19
Angular spread at Tx [degree]	10.23	10.32	11.96	15.31	2.68	2.71
Angular spread at Rx [degree]	11.04	11.14	60.76	59.80	2.71	2.74

the permeation coefficient when the permeation surface v has been permeated, and the diffraction coefficient when diffraction occurred on diffraction edge l. For rays where diffraction occurs, $s_{i,1}$ is the distance from the transmitting point to the first diffraction point and $s_{i,l}$ is the distance from the $(l-1)$-th diffraction point to the l-th point. For rays where diffraction does not occur, $s_{i,1}$ is the distance from the transmitting point to the receiving point. Also, $g_{n_t}(i)$ and $g_{n_r}(i)$ express the complex amplitude gain of the transmitting and receiving antennas in regards to the i-th ray, and k is the wave number.

3.3. Analysis results of path characteristics

First, we evaluate propagation channel characteristics based on differences in the maximum number of diffractions. Table 3 shows propagation simulation results when the maximum number of diffractions are changed, from Models 1 to 3. These are the results for the first transmitting antenna (Tx#1) and first receiving antenna (Rx#1) at the initial communication positions (Model 1 and Model 3 are for locations 40 m distant from the intersection, while Model 2 is for a location 5 m distant).

From Table 3, we could confirm that, while there is a slight difference between the Model 2 delay spread and the Tx angular spread, the propagation characteristics were virtually unchanged for all models overall even when the maximum number of diffractions increased. This is because the received level of the path for two diffractions is so small that the paths for zero or one diffraction generally dominate. As a result, we decided for future simulations to fix the number of diffractions to one diffraction.

Next, we conduct a performance evaluation for the maximum number of reflections. Tables 4 to 6 show the propagation simulation results when the maximum reflection coefficient is changed in Models 1 to 3. These tables, as well, show the results of Tx#1 and Rx#1 in the initial communication positions.

Figures 5 to 7 show the receiving angle profile between Tx#1 and Rx#1 in the initial communication positions, for Models 1 to 3, respectively. Note that these are Case 2, where the number of reflections is set at two reflections. The horizontal axis in the figures shows the arrival angle in the horizontal direction, with the vehicle's forward motion direction set at 0°, and leftward rotation from the forward direction until it reaches the vehicle rear direction is from 0° to 180°, while the rightward rotation is expressed as coordinates from 0° to −180°.

Figure 8 shows the simulation result examples between Tx#1 and Rx#1 in the initial communication positions for Models 1 to 3 (for Case 2).

Tables 4 and 5 reveal that the arrival angular spread for the receiving vehicle in Model 2 is larger than that for Model 1. This is due to the fact that the initial position of the receiving vehicle in Model 1 is 40 m from the intersection, while the position in Model 2 is 5 m, with the result that the angle of arriving radio wave is spread farther. In addition, when we confirm the receiving angular profiles in Figs. 5 and 6, we can see that the one in Model 2 has a larger spread. In fact, this can be confirmed from the simulation result example in Fig. 8.

From Table 6, the arrival angular spread of Model 3 is extremely small compared to that of Models 1 and 2, and the average receive level holds at a fixed value even if the number of reflections is increased. The reason for this is as follows. Model 3 is a model that takes the direct permeation

Table 4. Propagation simulation results at the intersection (Model 1)

Simulation condition	Case 1	Case 2	Case 3	Case 4
Maximum number of reflections	1	2	3	4
Total number of paths	16	36	64	99
Average receive level [dBm]	−105.9	−99.1	−98.4	−98.0
Delay spread [ns]	14.98	16.14	17.72	19.30
Angular spread at Tx [degree]	10.23	13.55	15.66	16.77
Angular spread at Rx [degree]	11.04	13.82	15.73	16.91

Table 5. Propagation simulation results at the intersection (Model 2)

Simulation condition	Case 1	Case 2	Case 3	Case 4
Maximum number of reflections	1	2	3	4
Total number of paths	20	61	141	211
Average receive level [dBm]	−84.1	−80.1	−73.6	−73.0
Delay spread [ns]	10.25	10.32	10.66	12.24
Angular spread at Tx [degree]	11.96	16.80	23.12	26.23
Angular spread at Rx [degree]	60.76	50.23	49.00	49.91

Table 6. Propagation simulation results at the intersection (Model 3)

Simulation condition	Case 1	Case 2	Case 3	Case 4
Maximum number of reflections	1	2	3	4
Total number of paths	17	37	65	100
Average receive level [dBm]	−76.6	−76.6	−76.6	−76.6
Delay spread [ns]	4.15	5.38	6.06	6.70
Angular spread at Tx [degree]	2.68	3.44	3.74	3.99
Angular spread at Rx [degree]	2.71	3.54	3.88	4.16

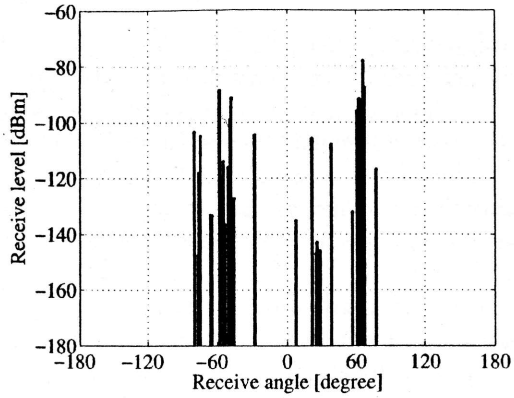

Fig. 6. Angular profile of Rx (Tx#1–Rx#1, Model 2, Case 2).

path into consideration, and the receiving level (–76.6 dBm) for this permeation path is larger by more than 20 dB than the average receiving level (–99.2 dBm) of the other reflection and diffraction waves. This can be confirmed by the permeation path of the spectrum shown at the arrival direction of –48.8 degrees in Fig. 6. As a result, in Model 3 this permeation path is extremely dominant. The angular spread is smaller, and the permeation path receiving level is fixed regardless of the number of reflections, so that the average receiving level is the same receiving level.

From Tables 4 to 6, we could confirm that the results of Cases 3 and 4, as with the evaluation for the maximum number of diffractions, while exhibiting a slight difference with the Model 2 delay spread and the Tx angular spread, the characteristics were virtually unchanged for all models overall. Therefore, we concluded that setting the maximum number of reflections at three is sufficient to model the

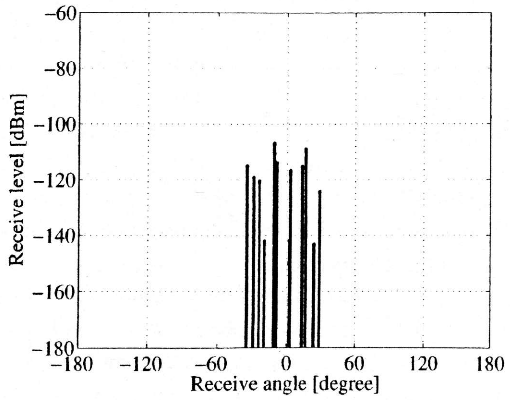

Fig. 5. Angular profile of Rx (Tx#1–Rx#1, Model 1, Case 2).

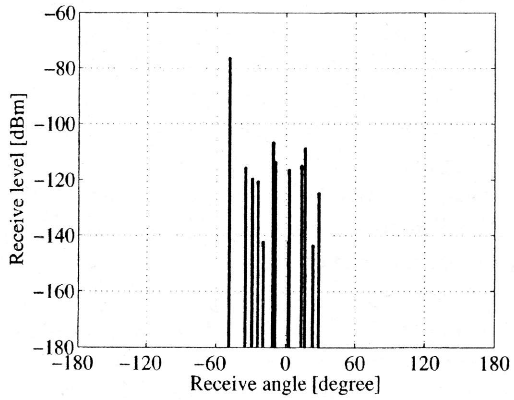

Fig. 7. Angular profile of Rx (Tx#1–Rx#1, Model 3, Case 2).

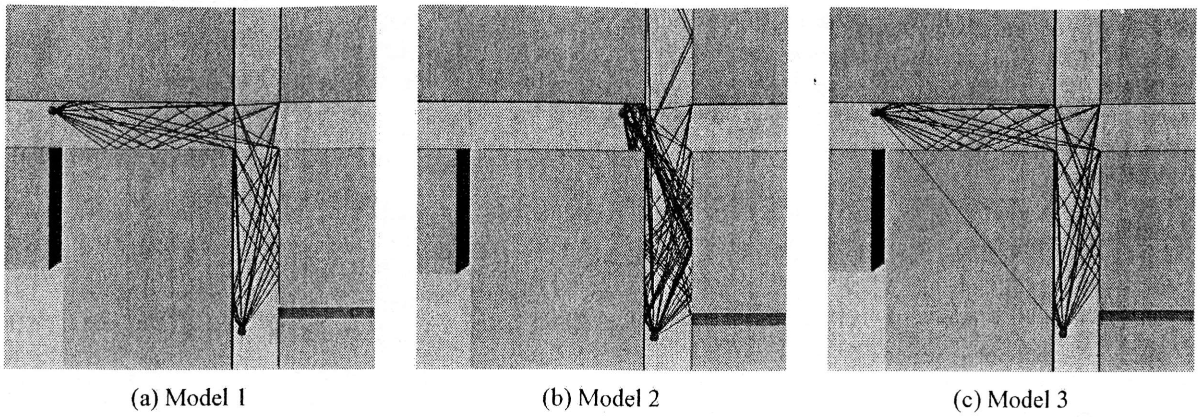

Fig. 8. Propagation simulation result (Tx#1–Rx#1, Case 2).

propagation channel characteristics in the intersection model.

3.4. Channel correlation analysis results

Next, we evaluate the correlation characteristics of the intersection propagation channel. For our evaluation measure, we used the complex spatial correlation coefficient $\rho_i(\Delta x)$ in the i-th receiving antenna. Here we define $\rho_i(\Delta x)$ as follows:

$$\rho_i(\Delta x) = \sum_{j=1}^{2} h_{ij}^{*}(x) h_{ij}(x + \Delta x) \times \left(\sum_{j=1}^{2} |h_{ij}(x)|^2 \sum_{j=1}^{2} |h_{ij}(x + \Delta x)|^2 \right)^{-1/2} \quad (7)$$

Here $h_{ij}(x)$ is the propagation channel response characteristics between the i-th receiving antenna and j-th transmitting antenna at position x. $h_{ij}(x + \Delta x)$ shows the propagation channel response characteristics in the position moved by exactly Δx from position x. Here if we assume that Δx_{Tx} and Δx_{Rx} represent the move distance for the transmitter and receiver, respectively, then in the current simulation, both the transmitter and receiver have moved at the same movement speed, so that $\Delta x = \Delta x_{\mathrm{Tx}} = \Delta x_{\mathrm{Rx}}$.

First, to investigate the relationship between the maximum number of reflections and the spatial correlation characteristics, we plotted the real number values of the complex spatial correlation coefficient $\rho_{\#1}(\Delta x)$ in receiving antenna #1, in relation to the movement distance Δx value normalized by the transmission wavelength λ ($\Delta x/\lambda$), for the results of Cases 1 to 3, using the symbols ○, △, and *, respectively (for Model 2). While the actual simulation was performed at a transmission frequency of 6 GHz, it was expressed by normalizing with wavelength λ, since the same results were obtained at 2 GHz. We also confirmed that the same results were obtained with receiving antenna #2.

From Fig. 9, since the receiving angular spread is large in Model 2, the amount of phase change in the range where the $\Delta x/\lambda$ value is large varies depending on the maximum number of reflections. In short-distance movement ranges, however (for example, when $\Delta x/\lambda$ is from 0 to 0.2), we can see that the amount of phase change shows virtually no difference even when the maximum number of reflections is changed. We confirmed that the same results were obtained in Models 1 and 3, as well. Next, we evaluate the differences in the spatial correlation characteristics of each model.

Figure 10 shows the complex element spatial correlation coefficient $\rho_{\#1}(\Delta x)$ in receiving antenna #1 in relation to $\Delta x/\lambda$ (for Case 2). In this figure, the results of Models 1 to 3 show absolute values with a dotted line, solid line, and dashed line, respectively, with the real number values plotted using the symbols ○, △, and *, respectively.

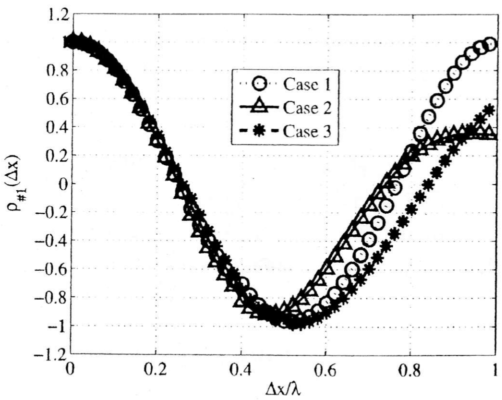

Fig. 9. Spatial correction analysis results for maximum number of reflections (Model 2).

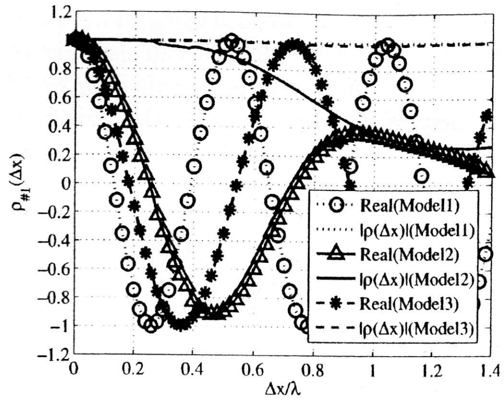

Fig. 10. Spatial correlation analysis results for the intersection models (Case 2).

In Fig. 10, the real number value for $\rho_{\#1}(\Delta x)$ changes greatly in relation to the $\Delta x/\lambda$ values. This is because movement of the transmitter and receiver toward the road intersection causes the propagation path length to shorten, resulting in a phase rotation. Regarding the absolute value of $\rho_{\#1}(\Delta x)$, however, the absolute values of Models 1 and 3 remained virtually unchanged, while that of Model 2 changed sharply. This was because the Model 2 receiving angular spread is large.

Meanwhile, focusing on the short movement distance in Fig. 10 (for example, when $\Delta x/\lambda$ is from 0 to 0.2), the absolute value of $\rho_{\#1}(\Delta x)$ for all models was generally about 1, so that a phase rotation only occurred. While not shown in the figure, we confirmed that the same trend seen for real numbers also occurred for imaginary numbers. We found, however, that the amount of rotation differed depending on the model. In Model 1, where the direction of radio wave arrival is the vehicle's direction of forward motion and where the angular spread is small, the amount of phase rotation is large, with phase rotation covering just the amount of change in wavelength corresponding to the movement distances of the transmitting and receiving terminals. This has also been confirmed in Ref. 9.

By contrast, in Model 2 with its large angular spread, and in Model 3 with its dominant direction of radio wave arrival coming at an angle from the vehicle's direction of forward motion, the amount of phase rotation was smaller.

3.5. Discussion

We here summarize the ray-tracing simulation results of propagation characteristics. In intersections without line-of-sight, we found that communication when both the transmitter and receiver are proceeding in the direction of the road intersection shows changes in propagation channel characteristics due to phase rotation at short movement distances. Therefore, if we assume that the transmitter's and receiver's positions are x_{Tx} and x_{Rx}, respectively, and movement distances are Δx_{Tx} and Δx_{Rx}, the following approximation formula is obtained:

$$\mathbf{H}(x_{\mathrm{Tx}} + \Delta x_{\mathrm{Tx}}, x_{\mathrm{Rx}} + \Delta x_{\mathrm{Rx}}) \simeq \mathbf{H}(x_{\mathrm{Tx}}, x_{\mathrm{Rx}}) \exp(j\theta) \tag{8}$$

Note that the $\exp(j\theta)$ value changes depending on the arrival, the radiation angle, and the size of angular spread.

4. Intersection Propagation Modeling

Based on the propagation characteristic evaluation results of the previous section, we now perform intersection propagation modeling. While a difference in the receiving angular spread exists between Models 1 and 2, we can still summarize both of their environments as having multi-paths with about the same receiving levels.

For Model 3, however, while the receiving angular spread is small, the environment includes just one path with a large receiving level.

Modeling is possible based on these models, as shown in Figs. 11 and 12. Figure 11 corresponds to the situations in Models 1 and 2, forming an environment of reflection and diffraction waves only, without any permeated objects existing nearby. We believe that this model would still apply even in cases where vehicles (buses, trucks, etc.) block the front side of the receiving vehicle. The reason is that, while the dominant radio wave arrival direction is at an angle to the forward motion of the receiving vehicle because the forward direction is blocked, there would still exist multi-paths at about the same receiving level. In this case, the angular spread for both the transmit-

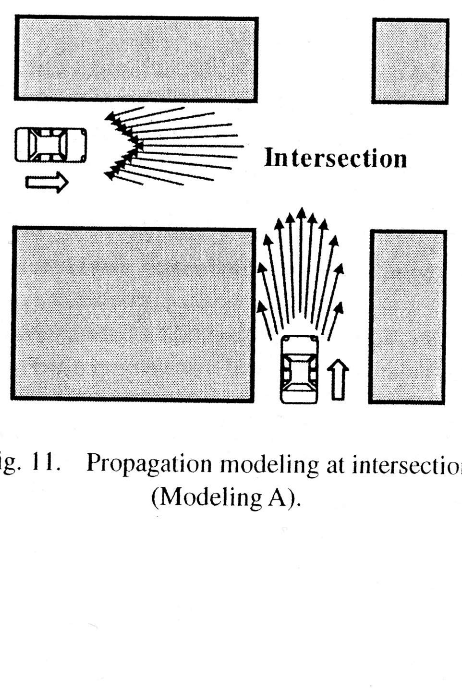

Fig. 11. Propagation modeling at intersection (Modeling A).

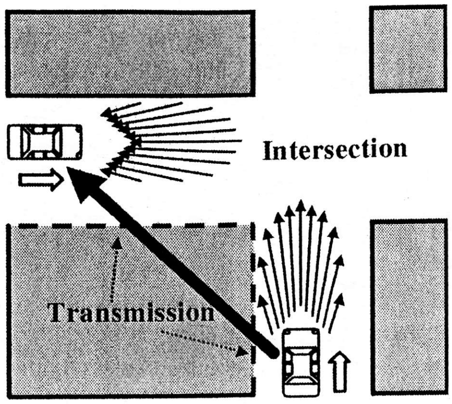

Fig. 12. Propagation modeling at intersection (Modeling B).

ting and receiving sides, the number of paths, the dominant arrival (reflection) direction, etc., are expressed as parameters.

Figure 12, meanwhile, corresponds to the Model 3 case, for a situation where permeation objects exist in the intersection, and form an environment with an extremely high level of permeation paths. In this case, we can express as parameters the relatively high intensity of permeation paths compared to the reflection and diffraction waves. Moreover, the case where the permeation paths are at about the same receiving level as the reflection and diffraction waves can be incorporated into the Fig. 11 model.

In this kind of intersection environment, environments with completely blocked visibility can be modeled with Fig. 11, while cases where permeation objects exist between the transmitting and receiving points can be modeled with Fig. 12.

5. Decision Feedback Channel Estimation Method

Based on the characteristics of intersection propagation channels found in the previous sections, we propose a MIMO-STBC method applicable to IVC. While the approximation method in Eq. (8) establishes both of the propagation models shown in Figs. 11 and 12, this value can vary greatly depending on the angular spread and on the relative intensity of the permeation path to the reflection and diffraction paths. As a result, it is unable to settle on a value for the amount of phase rotation corresponding to the movement distance obtained from vehicle speed, etc., as in Ref. 9.

Therefore, we propose the decision feedback channel estimation method. The proposed method performs complete control of the receiver only. First, we make a decision signal on the receiver decoded using STBC. Next, we feed back the decision signal, and calculate the amount of change $\exp(j\theta)$ of the propagation channel.

Here we define the receiving signal vector $\mathbf{R}_i(m_0)$ for the discrete time $2m_0$ and $2m_0+1$ intervals in the i-th receiving antenna.

$$\mathbf{R}_i(m_0) = \begin{bmatrix} y_i(2m_0) \\ y_i(2m_0+1) \end{bmatrix} \tag{9}$$

If we assume that the propagation channel in time t_0 was accurately estimated, then $\hat{\mathbf{H}} = \mathbf{H}(t_0)$, and h_{i1}, h_{i2} can be handled as if already known. If we assume, however, that in reality signals are received at the $2m_0$ and $2m_0+1$ intervals during time $t_0+\Delta t$, then

$$\mathbf{R}_i(m_0) = \mathbf{G}_2(m_0) \begin{bmatrix} \tilde{h}_{i1} \\ \tilde{h}_{i2} \end{bmatrix} \tag{10}$$

and encoding interference occurs due to changes in the propagation channel over time. Therefore, to convert the approximation formula (8) to a time function, we next assume that distances Δx_{Tx} and Δx_{Rx} were covered during time Δt, which can be expressed as follows:

$$\mathbf{H}(t_0+\Delta t) \simeq \mathbf{H}(t_0)\exp(j\theta) \tag{11}$$

As a result, Eq. (10) can be transformed as follows:

$$\mathbf{R}_i(m_0) \simeq \mathbf{G}_2(m_0) \begin{bmatrix} h_{i1} \\ h_{i2} \end{bmatrix} \exp(j\theta) \tag{12}$$

Here when the Δt value is small, the effects of encoding interference are also small, and we can assume that STBC decoding proceeds relatively accurately. In other words, if we use $\hat{\mathbf{H}}$ so that the signals $s(2m_0)$ and $s(2m_0+1)$ after decoding by STBC are $s'(2m_0)$ and $s'(2m_0+1)$, respectively, they can be expressed as follows. (Note, however, that this assumes the number of receiving antennas $N_r = 2$.)

$$\begin{aligned} s'(2m_0) = \sum_{i=1}^{N_r} \Big\{ & \left(h_{i1}^*\tilde{h}_{i1} + h_{i2}\tilde{h}_{i2}^*\right) s(2m_0) \\ & + \left(h_{i1}^*\tilde{h}_{i2} - h_{i2}\tilde{h}_{i1}^*\right) s(2m_0+1) \Big\} \end{aligned} \tag{13}$$

$$\begin{aligned} s'(2m_0+1) = \sum_{i=1}^{N_r} \Big\{ & \left(h_{i1}\tilde{h}_{i1}^* + h_{i2}^*\tilde{h}_{i2}\right) s(2m_0+1) \\ & + \left(h_{i2}^*\tilde{h}_{i1} - h_{i1}\tilde{h}_{i2}^*\right) s(2m_0) \Big\} \end{aligned} \tag{14}$$

From these two formulas, we can confirm that encoding interference arises from the change in the propagation channel over time. We therefore temporarily conclude that the two signals are correct. To ensure that $s'(2m_0)$ and $s'(2m_0 + 1)$ are at the same signal amplitude as $s(2m_0)$ and $s(2m_0 + 1)$, we set the normalized signals to $\hat{s}(2m_0)$ and $\hat{s}(2m_0 + 1)$. If we feed back these decision signals, and calculate the STBC matrix $\hat{\mathbf{G}}_2(m_0)$, we obtain

$$\hat{\mathbf{G}}_2(m_0) = \begin{bmatrix} \hat{s}(2m_0) & \hat{s}(2m_0+1) \\ -\hat{s}^*(2m_0+1) & \hat{s}^*(2m_0) \end{bmatrix} \tag{15}$$

In addition, for the case where the effects of encoding interference are assumed to be small and STBC decoding was accurate, the following formula is established:

$$\hat{\mathbf{G}}_2(m_0) = \mathbf{G}_2(m_0) \tag{16}$$

This result means that $\mathbf{R}_i(m_0)$, $\mathbf{G}_2(m_0)$, h_{i1}, and h_{i2} in Eq. (12) can be handled as if already known, and the two $\exp(j\theta)$ values can be calculated, and these results are represented by $\alpha_{1,i}$ and $\alpha_{2,i}$:

$$\alpha_{1,i} = \frac{y_i(2m_0)}{\hat{s}(2m_0)h_{i1} + \hat{s}(2m_0+1)h_{i2}} \tag{17}$$

$$\alpha_{2,i} = \frac{y_i(2m_0+1)}{-\hat{s}^*(2m_0+1)h_{i1} + \hat{s}^*(2m_0)h_{i2}} \tag{18}$$

As seen here, a single STBC symbol interval ($2m_0$ and $2m_0 + 1$ intervals) for a single receiving antenna can be used to find two values. Therefore, we find the average α_{m_0} for all values found for the number of receiving antennas N_r:

$$\alpha_{m_0} = \frac{1}{N_r}\sum_{i=1}^{N_r}\left(\frac{\alpha_{1,i} + \alpha_{2,i}}{2}\right) \tag{19}$$

Furthermore, if we average α_{m_0} over the multiple symbol interval m_{ave}, and call that value α_{ave} (m_{ave} has a multiple of 2), then we obtain

$$\alpha_{ave} = \frac{1}{m_{ave}}\sum_{m_{ave}} \alpha_{m_0} \tag{20}$$

Using this α_{ave} to calculate the new channel estimation matrix $\hat{\mathbf{H}}_{new}$, it is expressed as follows:

$$\hat{\mathbf{H}}_{new} = \alpha_{ave}\hat{\mathbf{H}} \tag{21}$$

Setting $\hat{\mathbf{H}}_{new}$ as $\hat{\mathbf{H}}$, we use it in STBC decoding in the next m_{ave} symbol interval. Thereafter, by renewing the channel estimation matrix for each m_{ave} symbol interval, we can track changes in the propagation channel.

6. Computer Simulation

To investigate the validity of the proposed method, we did a performance comparison with a method that does not perform propagation channel estimation correction (a method that does not track propagation channel changes as movement occurs). For the computer simulation, we used the QPSK modulation method.

6.1. Simulation conditions and statistical evaluation method

In this paper, we assume that, at the initial communication position (time t_0), accurate propagation channel estimation can be performed [$\hat{\mathbf{H}} = \mathbf{H}(t_0)$], and then perform evaluation of propagation characteristics in regards to phase change in the propagation channel that occurs with later movement. For the propagation channels, we targeted the case where the maximum number of reflections is two (Case 2). We chose this number because, from the propagation characteristic evaluation results in Section 3 (Fig. 9), we found that when the range of movement distances is short (for example, when $\Delta x/\lambda$ is from 0 to 0.2) there is virtually no difference in the amount of phase change even when the maximum number of reflections is changed from one reflection to three.

For the propagation simulation, we decided to make the phases for all paths unique, since the initial phase for each path is fixed. In reality, however, the phases should be randomly distributed because of slight differences in the angles of reflection surfaces or shifts in the vehicle running lane positions, etc. Therefore, for a statistical evaluation method, we applied the following method. First of all, for the first simulation round, we set the vehicle to a fixed movement speed, and transmitted 30 symbols over the movement distance at intervals of 0.5 mm. Then, we used a method that implements uniform random numbers for 10,000 rounds to randomize the initial positions of each path. This action statistically handles the effects of phasing. In addition, we set the m_{ave} values in the decision feedback channel estimation method to 30 symbols. Furthermore, to achieve changes in the propagation channel related to vehicle movement, we conducted a propagation simulation using the ray-tracing method for each vehicle movement of 0.5 mm, to regenerate the paths.

6.2. Performance evaluation in Modeling A

For Modeling A, we targeted the Model 1 and Model 2 propagation simulation results in Section 3 that took into account the reflection and diffraction paths only.

To evaluate the characteristics versus SNR, Figs. 13 and 14 show the Bit Error Rate (BER) for the SNR in Models 1 and 2, respectively. The figures show the plots for $\Delta x/\lambda$ = 0.03, 0.04, and 0.05 (represented by *, ○, and △, respectively). In these figures, the dotted line represents a method that does not perform any propagation channel estimation correction, while the solid line represents the proposed method. In addition, the BER for the SISO (Single-Input Single-Output) case where communication is performed by single transmitting and receiving elements is shown by the dashed line and by ▽ (this assumes that all transmitting power is a fixed value, using Tx#1 and Rx#1). For reference, since Models 1 and 2 are in environments with multiple arrivals of paths at about the same receiving level, the theoretical value for BER characteristics of single-element QPSK synchronous detection in a Rayleigh fading environment is shown in the dashed line only.

From Figs. 13 and 14, we can see that the method that does not perform any propagation channel estimation correction exhibited deteriorating characteristics versus SNR as $\Delta x/\lambda$ grew larger. By contrast, the proposed method obtained fixed and high-quality characteristics regardless of $\Delta x/\lambda$. This result was due to the nonoccurrence of encoding interference, which was due to the steady renewal of channel estimation. In addition, a comparison of the two figures reveals that the deterioration in characteristics shown by the method that does not perform any propagation channel estimation correction was smaller in Model 2 than in Model 1. This was due in Model 1 to the small angular spread of the receiving vehicle's radio wave arrival and to the dominance of the vehicle's forward motion, whereas in Model 2 the angular spread was larger and the amount of change in propagation characteristics corresponding to the vehicle's direction of motion was smaller.

Furthermore, in Fig. 13, for the case of $\Delta x/\lambda = 0.05$, we saw that the BER for the method not performing propagation channel estimation correction showed more deterioration than SISO. In other words, the SNR's improvement capability provided by MIMO was lost due to vehicle movement.

We also learned from these figures that the BER characteristics for SISO show virtually the same results as the theoretical characteristics in the Rayleigh fading environment. From these results, we conclude that the Modeling A environment modeled in this simulation has characteristics close to the Rayleigh fading environment.

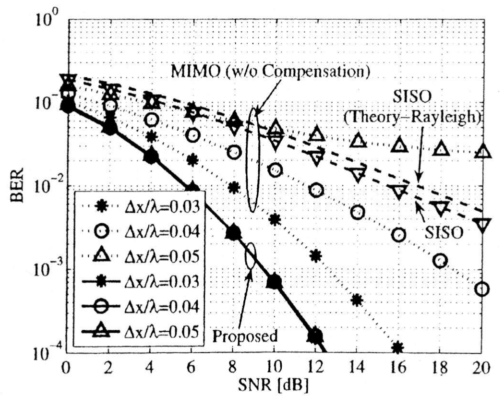

Fig. 13. BER performance versus SNR (Model 1, QPSK modulation).

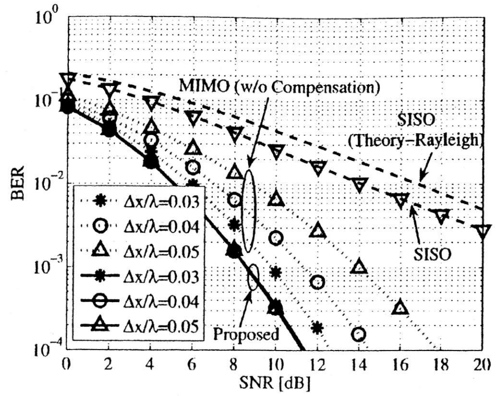

Fig. 14. BER performance versus SNR (Model 2, QPSK modulation).

As can be seen from the above, we confirmed that the proposed method can obtain stable, high-quality characteristics regardless of the size of the angular spread in a Rayleigh fading environment.

6.3. Performance evaluation in Modeling B

For Modeling B, we used the propagation simulation results for Model 3 that took into consideration the direct permeation path in Section 3. Figure 15 shows the BER versus SNR in Model 3. As in the previous section, we plotted for $\Delta x/\lambda = 0.03$, 0.04, and 0.05 (represented by *, ○, and △, respectively), with the dotted line representing a method that does not perform any propagation channel estimation correction and the solid line representing the

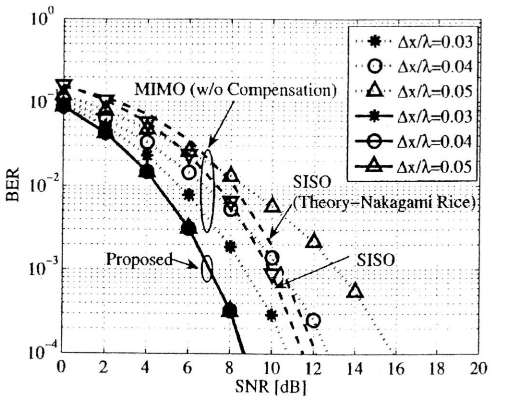

Fig. 15. BER performance versus SNR (Model 3, QPSK modulation).

proposed method. In addition, the BER for the SISO case is shown by the dashed line and by ∇. For reference, considering that Model 3 has one permeation path that is extremely dominant, the theoretical value for BER characteristics of single-element QPSK synchronous detection in a Nakagami-Rice fading environment is shown in the dashed line only. At this time, we referred to the simulation results in Section 3 for the receiving level ratio of the direct wave to the reflection and diffraction waves in the Nakagami-Rice environment, to obtain 22.6 dB.

From Fig. 15, we can see that, while the method that does not perform any propagation channel estimation correction exhibited deteriorating characteristics versus SNR as $\Delta x/\lambda$ grew larger, the proposed method showed absolutely no deterioration due to the $\Delta x/\lambda$ value. This was due to the same reason as seen for Modeling A. In addition, assuming a frequency of 5.8 GHz and a data packet length of 120 μs, then for $\Delta x/\lambda = 0.04$, we could confirm the validity of the proposed method at a normal running speed corresponding to a vehicle speed of about 62 km/h.

In addition, with the BER characteristics for SISO showing virtually the same results as the theoretical characteristics in the Nakagami-Rice fading environment, we conclude that the Modeling B environment has characteristics close to the Nakagami-Rice fading environment.

As can be seen from the above, we confirmed that the proposed method can always obtain fixed BER characteristics regardless of the movement distance or the transmission frequency, suppressing deterioration of characteristics due to movement.

Moreover, since the simulation results for this evaluation model satisfy the delay spread << symbol length (assumed to be about 1 μs) relationship, we can assert that it shows flat fading characteristics.

7. Conclusions

In this paper, we investigated an intervehicle communication (IVC) method that considers radio wave propagation conditions during IVC at intersections. First, we used the ray-tracing method to evaluate the characteristics of radio wave propagation in intersection models without line-of-sight, and performed propagation modeling. Then we proposed an IVC method based on MIMO-STBC that makes use of these characteristics. As a result, we obtained constantly fixed bit error rate characteristics, regardless of the movement distance or the transmission frequency, confirming its validity. In addition, we confirmed that the transmission modeling result virtually matches the characteristics of the Rayleigh fading environment and the Nakagami-Rice fading environment.

As a first step of investigation, we hypothesized for this paper an intersection on office-lined streets with large numbers of vehicles, and implemented a basic investigation targeting point-to-point communication focusing on the characteristics of tracking changes in propagation channels as transmitter and receiver are in motion. However, in order to realize a safe driving support system that demands high reliability, we believe that targeting point-to-point communication should go beyond this basic investigation to include verification of effectiveness under various environments. Possible situations could include communication in suburban areas where wooden structures exist in the surrounding area, situations where the existence of blocking vehicles results in large differences in the receiving level or propagation characteristics between antenna branches, or situations that take into account reflection waves coming off of multiple vehicles.

Other issues for consideration include adaptive access control between multiple vehicles, and evaluation of characteristics in frequency selective fading environments.

REFERENCES

1. Chen W, Cai S. Ad hoc peer-to-peer network architecture for vehicle safety communications. IEEE Commun Mag 2005;43:100–107.
2. Gesbert D, Shafi M, Shiu D, Smith PJ, Naguib A. From theory to practice: An overview of MIMO space-time coded wireless systems. IEEE J Sel Areas Commun 2003;21:281–302.
3. Karasawa Y. MIMO propagation channel modeling. IEICE Trans Commun 2005;E88-B:1829–1842.
4. Kermoal JP, Schumacher L, Pedersen KI, Mogensen PE, Frederiksen F. A stochastic MIMO radio channel model with experimental validation. IEEE J Sel Areas Commun 2002;20:1211–1226.
5. Jensen MA, Wallace W. A review of antennas and propagation for MIMO wireless communications. IEEE Trans Antennas Propag 2004;52:2810–2824.
6. Alamouti S. A simple transmit diversity technique for wireless communications. IEEE J Sel Areas Commun 1998;16:1451–1458.
7. Seidel SY, Rappaport TS. Site-specific propagation prediction for wireless in-building personal communication system design. IEEE Trans Veh Technol 1994;43:879–891.
8. Imai T. Prediction of propagation characteristics in tunnels using ray-tracing method. Trans IEICE 2002;J85-B:216–226.
9. Ito K, Itoh N, Sanda K, Karasawa Y. Inter-vehicle communication scheme based on MIMO-STBC for propagation environment in intersection without line-of-sight. Inter symbol interference problem and its countermeasure in high speed mobile environment. Tech Rep IEICE 2005;A-P2005-108.

10. Mckeown MA, Cruickshank DGM, Lindsay IAB, Thompson MS, Farson SA, Hu Y. Carrie frequency offset estimation in BLAST MIMO systems. Electron Lett 2003;39:1752–1753.
11. Siemons F, Moeneclaey M. Computationally efficient frequency offset estimation for flat-fading MIMO channels: Performance analysis and training sequence design. Conf Rec IEEE GLOBECOM'04, Vol. 4, p 2460–2464.
12. Besson O, Stoica P. On parameter estimation of MIMO flat-fading channels with frequency offsets. IEEE Trans Signal Process 2003;51:602–613.
13. Shahbazpanahi S, Gershman AB, Giannakis GB. Joint blind channel and carrier frequency offset estimation in orthogonally space-time block coded MIMO systems. IEEE 6th Workshop on Signal Process Advances in Wireless Commun, p 363–367, 2005.
14. Barry JR, Batra A. A multidimensional phase-locked loop for blind equalization of multi-input multi-output channels. Conf Rec IEEE ICC96, Vol. 3, p 1307–1312.
15. Tarokh V, Jafarkhani H. A differential detection scheme for transmit diversity. IEEE J Sel Areas Commun 2000;18:1169–1174.
16. Radio Propagation Laboratory -RapLab-, http://www4.kke.co.jp/raplab/
17. Hosoya Y (general editor). Radio propagation handbook. Realize Press; 1999.
18. Erceg V, Rustako J, Roman RS. Diffraction around corners and its effects on the microcell coverage area in urban and suburban environments at 900 MHz, 2 GHz, and 6 GHz. IEEE Trans Veh Technol 1994;43:762–766.

AUTHORS (from left to right)

Kenji Ito (member) received his B.S. and M.S. degrees in electrical and computer engineering from Nagoya Institute of Technology in 1999 and 2001 and joined Toyota Central Research and Development Laboratories, Inc. His research interests include terrestrial digital broadcasting and mobile radio systems such as MIMO. He received a Research Award from the IEICE Technical Committee and Communication Quality in 2001. He is a member of IEEE.

Nobuo Itoh (member) received his B.E. and M.E. degrees in electrical engineering from Fukui University in 1980 and 1982 and D.Eng. degree from Gifu University in 1995. He joined Toyota Central Research and Development Laboratories, Inc., in 1998. His research interests include digital signal processing for mobile communication systems. He is currently a senior researcher and laboratory manager of ITS Lab. I of Toyota CRDL. He is a member of IEICE and the Institute of Image Information and Television Engineers.

Katsushi Sanda received his B.S. and M.S. degrees from Nagoya University in 1998 and 2000 and joined Toyota Central Research and Development Laboratories, Inc. His research interests include digital signal processing for mobile communication systems. He is a member of the Information Processing Society of Japan.

AUTHORS (continued)

Yoshio Karasawa (member) received his B.E. degree from Yamanashi University in 1973 and M.S. and D.Eng. degrees from Kyoto University in 1977 and 1992. He joined KDD R&D Labs. in 1977. From 1993 to 1997, he was a Department Head of ATR Optical and Radio Communications Res. Labs. and ATR Adaptive Communications Res. Labs. Currently, he is a professor and director of the Advanced Wireless Communication Research Center at the University of Electro-Communications. Since 1977, he has engaged in studies on wave propagation and radio communication antennas, particularly on the theoretical analysis and measurements for wave-propagation phenomena, such as multipath fading in mobile radio systems, tropospheric and ionospheric scintillation, and rain attenuation. His recent interests are in frontier regions bridging "wave propagation" and "digital transmission characteristics" in wideband mobile radio systems such as MIMO. He received the Young Engineers Award from IEICE in 1983 and the Meritorious Award on Radio from the Association of Radio Industries and Businesses in 1998, a Research Award from the International Communications Foundation in 2006, and two Paper Awards from IEICE in 2006. He is a senior member of IEEE and a member of SICE.